

# RSC Medicinal Chemistry

Accepted Manuscript

This article can be cited before page numbers have been issued, to do this please use: A. Maturi, V. Pogaku, S. Kumar and M. Kim, *RSC Med. Chem.*, 2025, DOI: 10.1039/D5MD00397K.



This is an Accepted Manuscript, which has been through the Royal Society of Chemistry peer review process and has been accepted for publication.

Accepted Manuscripts are published online shortly after acceptance, before technical editing, formatting and proof reading. Using this free service, authors can make their results available to the community, in citable form, before we publish the edited article. We will replace this Accepted Manuscript with the edited and formatted Advance Article as soon as it is available.

You can find more information about Accepted Manuscripts in the [Information for Authors](#).

Please note that technical editing may introduce minor changes to the text and/or graphics, which may alter content. The journal's standard [Terms & Conditions](#) and the [Ethical guidelines](#) still apply. In no event shall the Royal Society of Chemistry be held responsible for any errors or omissions in this Accepted Manuscript or any consequences arising from the use of any information it contains.

## COMMUNICATION

## Hinge Binder Modification into Imidazopyridine for Targeting Actionable Mutations of RET Kinase

Received 00th January 20xx,  
Accepted 00th January 20xxArunkranthi Maturi<sup>1</sup>, Vinay Pogaku<sup>1</sup>, Surendra Kumar<sup>1</sup> and Mi-hyun Kim<sup>1,\*</sup>

DOI: 10.1039/x0xx00000x

The RET proto-oncogene plays a critical oncogenic driver in the development of several cancers. Despite the existence of clinically approved RET inhibitors, their limited response rates and the emergence of resistance due to diverse actionable mutations underscore the need for novel therapeutics. Herein, we report substituted imidazo[1,2-a]pyridine derivatives as new RET inhibitors exhibiting IC<sub>50</sub> values as low as 11 nM against three distinct point mutations and three important RET fusions. The binding mode and measured potency were elucidated by induced-fit docking simulations and the safety for cardiotoxicity was further evaluated.

## 1. Introduction

Rearranged during transfection (RET) is a receptor tyrosine kinase that activates cell signaling pathways, including PI3K/AKT and MAPK to lead to cell survival, proliferation, movement, and diversification.<sup>1</sup> The phosphorylation and activation of RET protein occur after ligand-independent homodimerization or binding interactions with ligands such as glial cell line-derived neurotrophic factor (GDNF).<sup>2</sup> However, RET alterations, such as comprising point mutations, gene fusions, gene loss, missense mutations in specific codons, amplification, and rearrangements, can lead to constitutive RET activation, bypassing these canonical mechanisms. Surely, altered RET proteins have been identified as oncogenic drivers of versatile solid cancers, including non-small cell lung cancer (NSCLC), differentiated thyroid cancer (DTC), papillary thyroid carcinoma (PTC), medullary thyroid cancer (MTC) metastatic, and colorectal cancer (mCRC).<sup>3,4,5,6,7</sup> Some of these alterations cause malignant cancers.<sup>4-8</sup> For example, a subset of patients with NSCLC harboring RET fusions presents low tumor mutational burden (TMB) and low programmed cell death protein-1 (PD-L1) expression ('cold tumor'), and respond poorly to immunotherapy.<sup>9,10</sup> Due to its clinical significance, the NCCN Clinical Practice Guidelines in Oncology have recommended RET as a biomarker for testing in NSCLC.<sup>11</sup> While some multi-kinase inhibitors and RET-selective inhibitors are clinically approved for RET-altered cancers, several key questions remain unanswered: Which actionable mutations are clinically meaningful? Why do some patients exhibit low response rates to RET inhibitors? How can future inhibitor design overcome drug resistance?<sup>12</sup> Among

the various reported RET alterations, RET-KIF5B is one of the most frequently observed oncogenic fusion genes, accounting for approximately 66% of RET fusions in NSCLC.<sup>7</sup> In contrast, RET-altered solid tumors other than NSCLC exhibit different fusion partner frequencies, with NCOA4 (32.6%) and CCDC6 (29.9%) predominant.<sup>7</sup> Point mutations are significant, not only as oncogenic drivers, but also as key determinants of drug resistance. While diverse point mutations have been reported, including gatekeeper, solvent front, gate wall, and P-loop mutations, gatekeeper (V804) and solvent front (G810) mutations have been reported in relation to drug sensitivity and acquired resistance.<sup>12-14</sup> Although pralsetinib and selpercatinib (**Figure 1**) have clinically demonstrated their superior selectivity and potency over earlier multi-kinase inhibitors,<sup>12,15</sup> the development of ideal molecular probes remains essential for elucidating the molecular mechanisms underlying actionable RET mutations and designing breakthrough drugs to address these mutations. For example, despite their effectiveness against RET<sup>V804M/L</sup> (gatekeeper mutation),<sup>16</sup> pralsetinib and selpercatinib presented significant limitations in addressing solvent front mutations and multiple alterations, posing significant clinical challenges. Therefore, we have modified the structures of RET hinge binders to overcome actionable RET alterations. To address these limitations, we previously modified the pyrazolopyridine hinge binder scaffold of selpercatinib into imidazopyridazine and introduced extended substituent at the 2<sup>nd</sup> and 6<sup>th</sup> positions of the hinge binder (**Figure 1**).<sup>12</sup> In this study, we explored the imidazopyridine scaffold, which contains fewer nitrogen atoms than imidazopyridazine. While increased aromatic nitrogens (N<sub>aro</sub>) in the hinge binder can enhance kinase-likeness,<sup>17,18</sup> they also increase hERG binding affinity or metabolic reactivity. To consider drug-likeness and drug efficacy, we selected one nitrogen atom that was neither involved in hydrogen bonding with the hinge region nor essential for facilitating synthetic chemistry. Furthermore, two structural variations of the imidazopyridine core were investigated: R<sub>1</sub> substituents at the 6-position and R<sub>2</sub> substituents at the 2-position (**Figure 1**). We elongated the imidazopyridine hinge binder with several privileged tails (aniline derivative) of known type II kinase inhibitors and compared their effects with that of a less-favoured tail.<sup>19,20</sup>

## 2. Results and discussion

<sup>a</sup> Gachon Institute of Pharmaceutical Science and Department of Pharmacy, College of Pharmacy, Gachon University, Yeonsu-gu, Incheon, Republic of Korea.

<sup>b</sup> \*Corresponding Author: kmh0515@gachon.ac.kr

## 2.1. Established synthetic routes of imidazopyridine derivatives

Compounds **9a–k** and **11a–c** were synthesized using the optimized **Scheme 1**. The reaction of ethyl 2-bromoacetate under neat conditions yielded compound **5**, which was then treated with phosphorus oxychloride ( $\text{POCl}_3$ ) to obtain compound **6**. Suzuki coupling reactions were then employed to synthesize intermediates **7a–h** and **10a–c**.<sup>21</sup> Iodination of

compound **7** produced the key intermediate **8a–h**, which was further subjected to Sonogashira coupling to furnish the desired compounds **9a–k**.<sup>22</sup> Compounds **11a–c** were synthesized via alkylation reactions (**Scheme 1**). The desired products **17a–d**, as well as compounds **19** and **20**, were synthesized using the elaborated **Scheme 2**. Cyclization was carried out using ethyl bromopyruvate under heating at  $110^\circ\text{C}$ , yielding compound **13**. Subsequently, iodination reaction was performed to produce compound **14b**, while **14a** was procured.

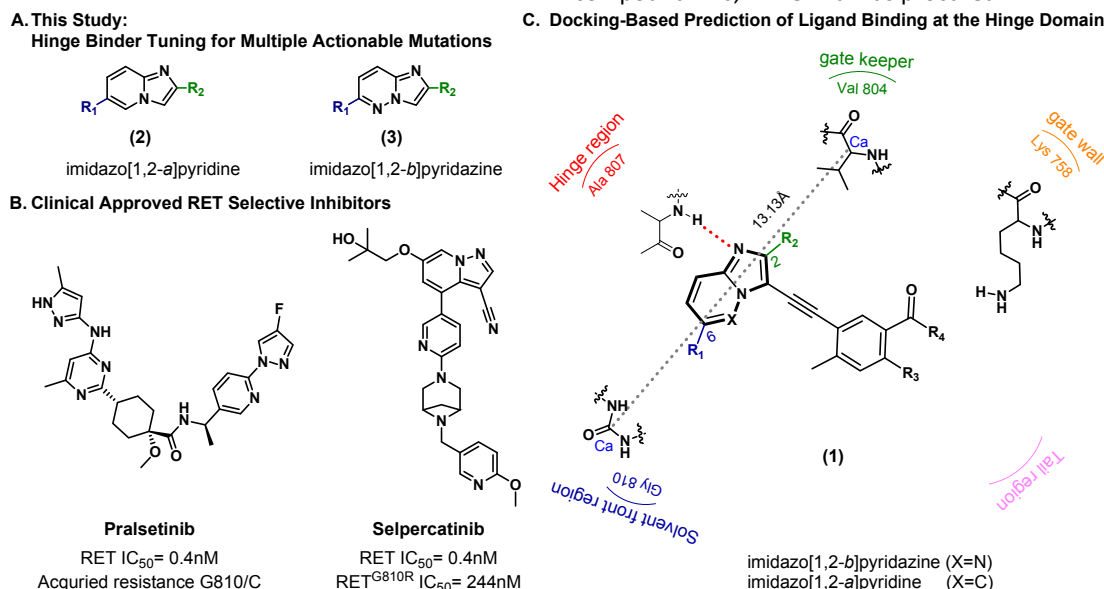
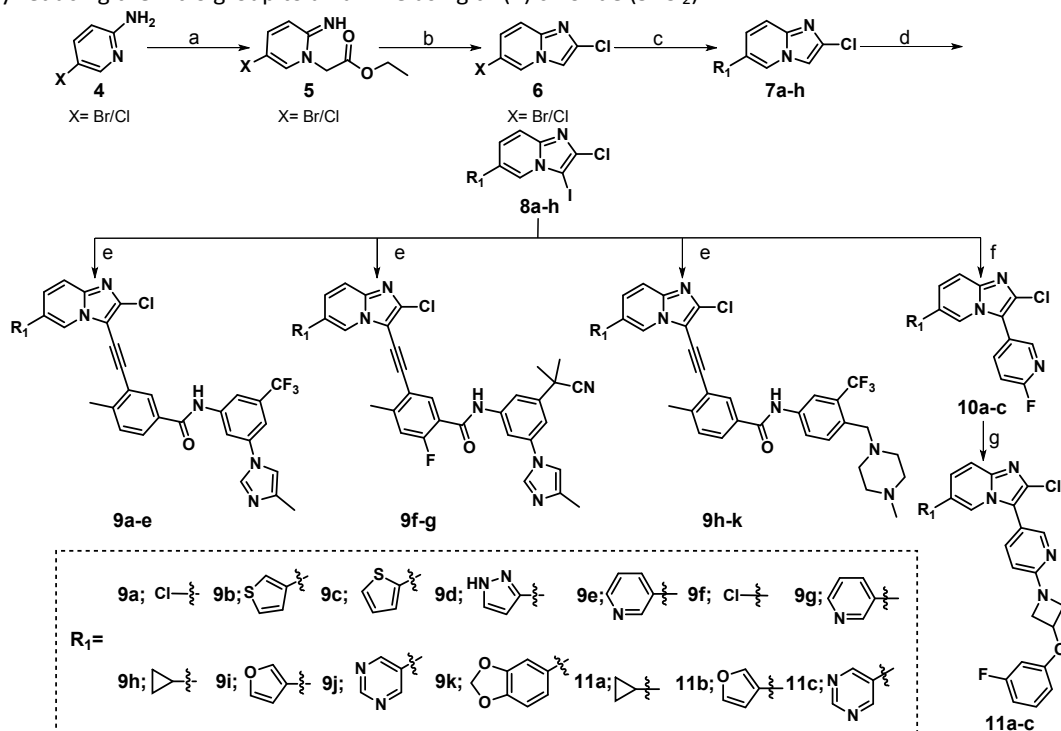
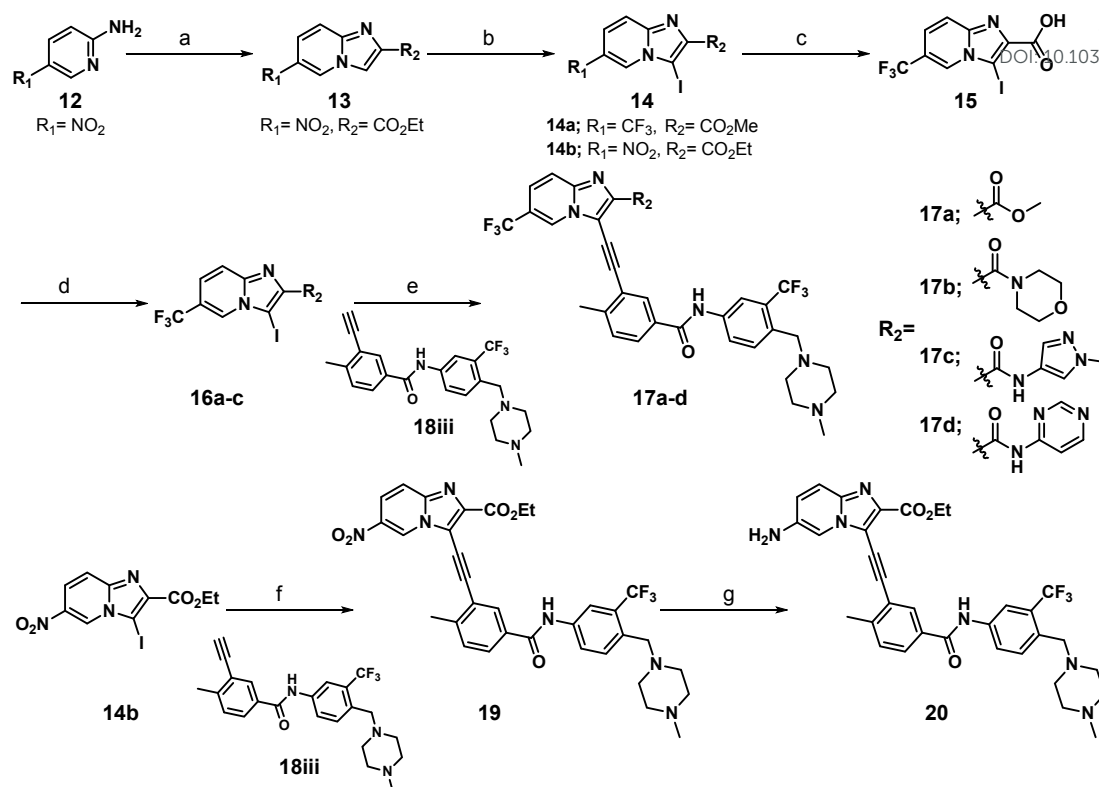


**Figure 1.** A. This study focuses on imidazole [1, a]pyridine Hinge Binder for Multiple Actionable Mutations. B. FDA-approved RET selective inhibitors. C. Computationally predicted binding interaction of the designed Hinge binder scaffolds

Hydrolysis of **14a** yielded acid **15**, which was then coupled with amines via acid-amine coupling to synthesize the key intermediates **16a–c**. Finally, Sonogashira coupling was employed to obtain the desired final compounds **17a–d** and **19**. Compound **20** was synthesized by reducing the nitro group to an amine using tin(II) chloride ( $\text{SnCl}_2$ ).<sup>23</sup>



**Scheme 1.** Synthesis of compounds **9a–k** and **11a–c**. Reaction conditions: a) Ethyl 2-bromoacetate, rt, 72.8%. b)  $\text{POCl}_3$ ,  $110^\circ\text{C}$ , 65%. c) Boronic acids and  $\text{K}_2\text{CO}_3$ ,  $\text{Pd}(\text{dppf})\text{Cl}_2$ ,  $90^\circ\text{C}$ , 12hrs, 60%. d) NIS, DMF, rt, 56.85%. e) 18i, 18ii, 18iii, cBRIDP,  $[(\text{cinnyl})\text{PdCl}]_2$ ,  $\text{Et}_3\text{N}$ , 2% TPGS/ $\text{H}_2\text{O}$ ,  $45^\circ\text{C}$ , THF, 51.7%. f)  $\text{Pd}(\text{dppf})\text{Cl}_2$ ,  $\text{K}_2\text{CO}_3$ ,  $90^\circ\text{C}$ , 12hrs, 60%. g) 4iv (amine),  $\text{K}_2\text{CO}_3$ , DMF,  $90^\circ\text{C}$ , 35%.



**Scheme 2.** Synthesis of compounds **17a–d**, **19**, and **20**. Reaction conditions: a) Ethyl bromopyruvate, rt, 60%. b) NIS, DMF, rt, 55%. c) THF: MeOH: H<sub>2</sub>O, rt, 50%. d) amine, DIPEA, T3P, CH<sub>2</sub>Cl<sub>2</sub>, 45%. e) cBRIDP, [(cinnyl)PdCl]<sub>2</sub>, Et<sub>3</sub>N, 2% TPGS/H<sub>2</sub>O, THF, 45°C, 45%. f) SnCl<sub>2</sub>, 70°C, 18%.

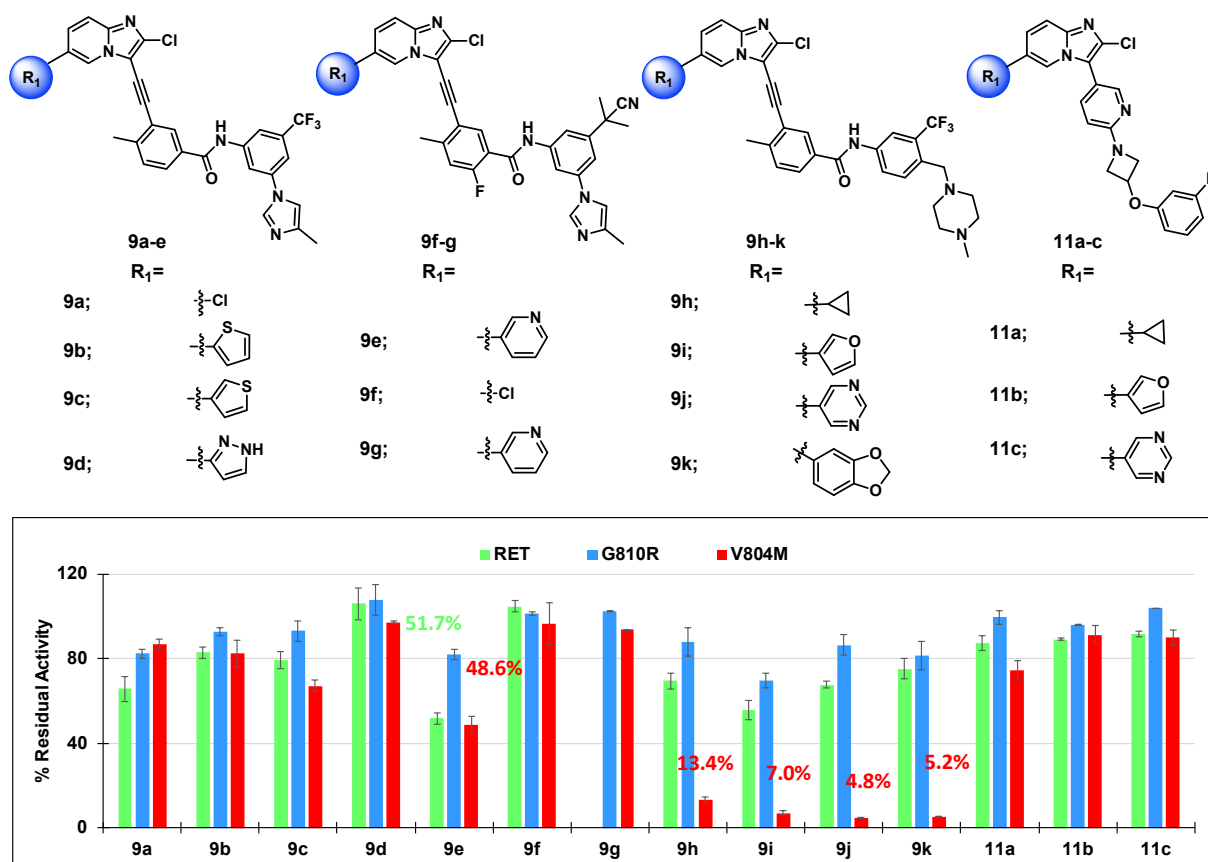
## 2.2. SAR screening of imidazopyridine derivatives

The R<sub>1</sub> and R<sub>2</sub> substituents were expected to be oriented toward the solvent front and gatekeeper region, respectively.<sup>12</sup> Therefore, for the systematic structure investigation of the imidazopyridine scaffold, the chloro group was initially fixed at the 2-position to obtain testing compounds with diverse R<sub>1</sub> substituents through facile and rapid synthesis (**Scheme 1**). Systematic modifications of the R<sub>1</sub> substituent was performed with privileged tail t<sub>1</sub> (of AMN-107),<sup>24</sup> resulting in compounds **9a–e**, including a chloro substituent (**9a**), thiophene substituents (**9b** and **9c**), pyrazole (**9d**), and pyridine (**9e**). Figure 2 shows a structure overview of the synthesized fourteen compounds **9a–k** and **11a–c**. RET panel screening at a single concentration demonstrated the preference of a heteroaryl group with a hydrogen-bonding acceptor (e.g., pyridyl group of compound **9e**, furan group of compound **9i** versus pyrazole group of compound **9d**).<sup>25</sup> Meanwhile, tested four tails presented the scope of this substituent effect. Retaining the pyridine group at the 6-position while changing the tail t<sub>2</sub> (compound **9g**), resulted in a notable reduction in RET inhibitory activity. Moreover, a fluorine atom was introduced into the aromatic ring of tail t<sub>2</sub> to modulate its electronic properties for SAR studies. Fluorine can act as a bioisostere or as part of a bioisosteric group, replacing lone pairs of electrons, hydrogen atoms, or methyl group, and can also mimic the functional properties of carbonyl, carbinol, and nitrile groups.<sup>26</sup> Even if we intended to restrict the conformation through the intramolecular F...H-N of the amide group, the pose of compound **9f–g** exhibited the interaction's trivial contribution to desirable bioactive conformation in our molecular docking simulations (**Figure S1–S4**). Various R<sub>1</sub> substituents were further combined with tail t<sub>3</sub>, thereby yielding compounds **9h–k**, and

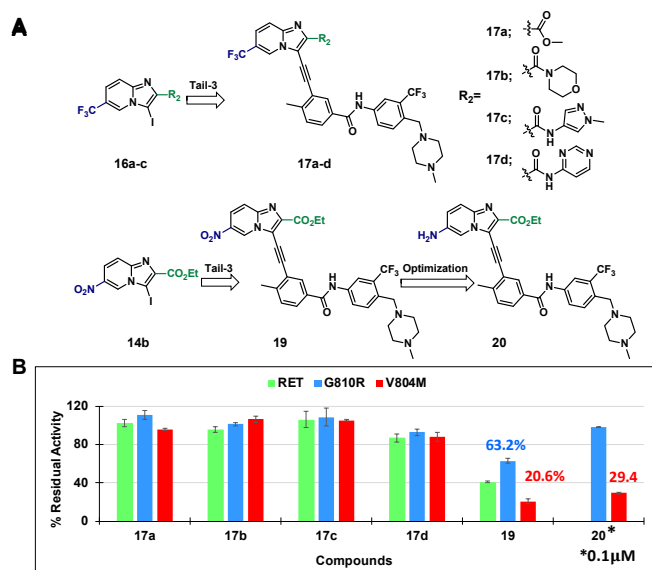
their inhibitory potencies against RET kinase were assessed. Surely, the compounds **11a–c** showed dramatically decreased RET inhibitory activities with the simple tail 4 compared to the privileged tails of type II kinase inhibitors (tail 1-3) shown in Figure 2.<sup>19,20</sup> The effective inhibition of the actionable mutant RET<sup>V804M</sup> encouraged us to further modify this hinge binder. Thus, we replaced the Cl group at the 6-position with CF<sub>3</sub> group and introduced various R<sub>2</sub> group (ester, cyclic tertiary amide, and secondary aryl amide group) into the 2-position.<sup>27</sup> We expected the CF<sub>3</sub> group to be well desolvated near the water front region to enhance the binding affinity with another actionable mutant RET<sup>G810R</sup>. Regrettably, all design attempts at the 2-position to occupy the small pocket near the gatekeeper residue, including compound **17c** benchmarked from the pyrazole amine of pralsetinib,<sup>28</sup> failed to demonstrate desirable kinase inhibitory activity (**Figure 3**, **Figure S6**). Subsequently, with the ester group fixed at the 2-position, we further investigated pharmacophores suitable for R<sub>1</sub> group at the 6-position. The comparable activities of compounds **9h–9k** suggested that the size of R<sub>1</sub> group did not make difference in the inhibitory activities. Therefore, the evidence encouraged us to introduce a small substituent at the 6-position exploring beyond heteroaryl groups. Concretely, the additional small R<sub>1</sub> groups (of -CF<sub>3</sub>, -NO<sub>2</sub>, -NH<sub>2</sub>) could be designed based on the context of priori screening using compounds **9a–k**. NO<sub>2</sub> group was introduced at the R<sub>1</sub> position instead of the CF<sub>3</sub> group, while maintaining the smallest R<sub>2</sub> substituent. Encouragingly, this replacement resulted in improved inhibitory activities against every RET panel (compound **17a** versus compound **19**). Therefore, the highly electron-withdrawing group was replaced with electron-donating NH<sub>2</sub> group to maintain hydrophilic property near water front region while increasing the electron

density of the bicyclic aromatic ring.<sup>29</sup> Compound **20**, containing NH<sub>2</sub> group, showed decreased inhibitory effect for RET<sup>G810R</sup> but maintained comparable to compound **19** for RET<sup>V804M</sup> inhibitory activity to compound **19** (Figure 3 & 4). The inhibitory potency values of compound **19** (-NO<sub>2</sub>) and **20** (-NH<sub>2</sub>) also gave additional knowledge, which the R<sub>1</sub> group at the 6-position can

be replaced with any hydrogen acceptor regardless of electron-rich or deficient. Based on the SAR study of the imidazopyridine derivatives, several promising compounds were selected for further testing against RET fusion mutations. Notably, compound **20** was the most active inhibitor for every RET fusion (Figure 4).<sup>30</sup>

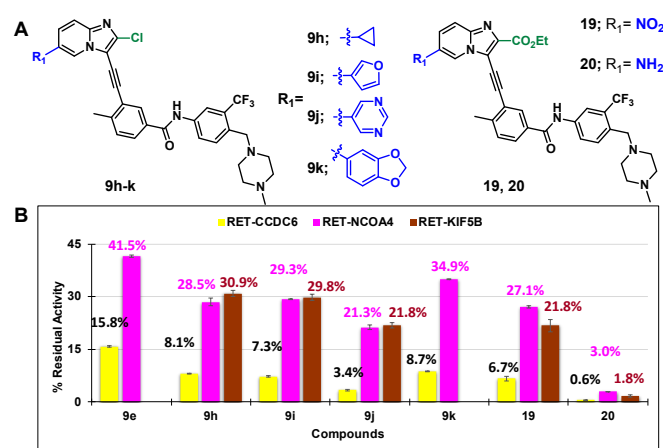


**Figure 2.** A. Imidazopyridine derivatives with four different types of tails exploring substituents directed towards R<sub>1</sub>. B. % Residual activity of the designed compounds at 1  $\mu$ M concentration (exceptionally, compound **9g**: 0.1  $\mu$ M) with RET kinases RET (green), G810R (blue), and V804M (red). Every activity value is shown in suppl. (Table S1)



**Figure 3.** A. Imidazopyridine derivatives with diverse substituents with tail t<sub>3</sub> **17a-d** and optimization of compound **19** and **20**. B. % Inhibition of the tested compounds against RET (gold), G810R (blue), and V804M (red). Testing concentration at 1  $\mu$ M (exceptionally, compound **20**: 0.1  $\mu$ M). Every activity value is shown in suppl. (Table S1).

### 2.3. Developability of imidazopyridine derivatives

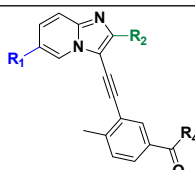
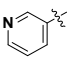
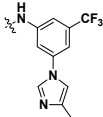
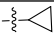
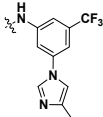
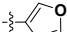
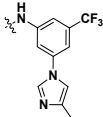
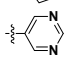
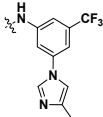
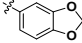
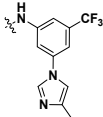


**Figure 4.** Exploration of R<sub>1</sub> group using chosen compounds. B. % Inhibition activity against RET fusions RET-CCDC6 (yellow), RET-NCOA4 (Magenta), and RET-KIF5B (brick red). Every activity value is shown in suppl. (Table S2). Testing concentration at 1  $\mu$ M.



Based on the preliminary screening results, we further investigated the imidazopyridine scaffold by evaluating selected promising derivatives for their inhibitory potencies ( $IC_{50}$ ) against representative actionable RET mutants ( $RET^{G810R}$  and  $RET^{V804M}$ ). Compound **9e** demonstrated moderate inhibitory potency of 0.8  $\mu M$  against the gatekeeper mutant ( $RET^{V804M}$ ) but exhibited the limited potency against the solvent front mutant ( $RET^{G810R}$ ) (Table 1). In contrast, compounds **9i–k** and **20** showed enhanced potency, displaying approximately two- to three-fold improvements over the  $RET^{V804M}$  mutant.

Table 1. Enzyme inhibition  $IC_{50}$  against  $RET^{V804M}$  &  $RET^{G810R}$  ( $\mu M$ ).

|  |   |                    |   |                                    |                      |
|---|---|--------------------|---|------------------------------------|----------------------|
| Entry   | R <sub>1</sub>  | R <sub>2</sub>     | R <sub>4</sub>  | Kinase assay IC <sub>50</sub> (μM) |                      |
|   |   |                    |   | RET <sup>V804M</sup>               | RET <sup>G810R</sup> |
| 9e  |    | Cl                 |  | 0.800                              | >10                  |
| 9h  |    | Cl                 |  | 0.011                              | 1.34                 |
| 9i  |    | Cl                 |  | 0.024                              | 3.11                 |
| 9j  |   | Cl                 |  | 0.017                              | 1.69                 |
| 9k  |  | Cl                 |  | 0.028                              | >10                  |
| 19  | NO <sub>2</sub>   | CO <sub>2</sub> Et |   | 0.044                              | 7.80                 |
| 20  | NH <sub>2</sub>   | CO <sub>2</sub> Et |   | 0.028                              | 0.96                 |

A radiometric biochemical assay.

Table 2. Therapeutic index assessment of representative RET kinase inhibitors against hERG toxicity.

| Entry     | Therapeutic ratio                      |  |
|-----------|--|--|
|           | $IC_{50}(hERG) / IC_{50}(RET^{V804M})$ | $IC_{50}(hERG) / IC_{50}(RET^{G810R})$ |
| <b>9e</b> | 37.50                                  | 3.00                                   |
| <b>9h</b> | 363.63                                 | 2.98                                   |
| <b>9i</b> | 174.16                                 | 1.34                                   |
| <b>9j</b> | 481.17                                 | 4.84                                   |
| <b>9k</b> | 142.85                                 | <1.0                                   |
| <b>19</b> | 60.90                                  | <1.0                                   |
| <b>20</b> | 167.85                                 | 4.89                                   |

hERG % residual activity and  $IC_{50}$  values are shown in Suppl. (Table S4).

Notably, compound **20** exhibited a significant enhancement, demonstrating up to a ten-fold increase in potency against the  $RET^{G810R}$  solvent front mutation. Structurally, these potent derivatives commonly feature electron-rich substituents and hydrogen bond acceptor atoms at the 6-position: a furan group in compound **9i**, a pyrimidine group in compound **9j**, and a benzodioxole moiety in compound **9k**. Interestingly, despite the

contrasting electronic features of the  $R_1$  substituents at this position, compound **19** containing the electron-withdrawing group maintained comparable potency to the electron-rich analogs. These results suggest that a hydrogen bond acceptor at the 6-position confers advantageous interactions against the gatekeeper mutation.<sup>25</sup> However, this beneficial effect was not maintained in the solvent front  $RET^{G810R}$  mutant (Table 1).<sup>31</sup> For further evaluation of our testing compounds, therapeutic ratios were determined to evaluate the safety profiles and guide future optimization of these imidazopyridine derivatives.<sup>32</sup> Compounds **9e**, **9i**, **9j**, **9k**, **19** and **20** demonstrated highly favorable therapeutic ratios against  $RET^{V804M}$ , indicating substantial potential for further development. For  $RET^{G810R}$ , the therapeutic ratios were relatively modest, indicating that further optimization is needed to improve safety margins.<sup>32</sup> These findings provide valuable insights into the SAR of this imidazopyridine series, emphasizing the importance of carefully balancing kinase targeting with hERG anti-targeting to mitigate an off-target toxicity.<sup>33</sup> Every experiment demonstrated that The Compound **20** is the best compound among the imidazopyridine series. Finally, the anti-proliferative effect of the compound **20** was further tested under NSCLC (Lc/2d cell lines having RET-CCDC6 fusion) to give the  $IC_{50}$  value of 5.3  $\mu M$  (Figure 5D). The double confirmation through the standard Cell Titer-Glo without any optimization of assay conditions suggests the biochemical potency of compound **20** is working and shows the potential for future drug discovery for RET alterations.<sup>34</sup>

## 2.4. Mode of action and Kinase Selectivity of the best compound

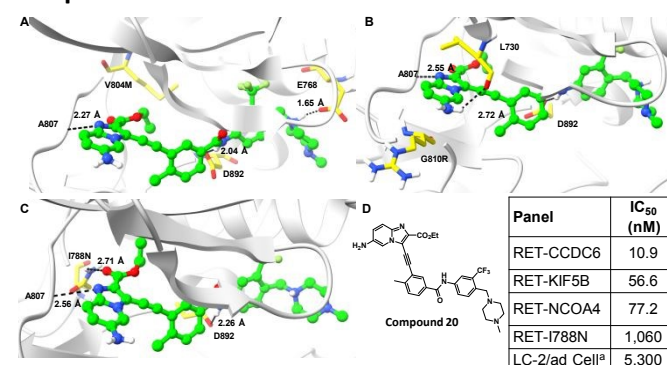


Figure 5. Molecular docking simulation of compound **20** along with the potency measurement against additional RET alterations. **A**. Best docking pose for  $RET^{V804M}$ ; **B**. Best docking pose for  $RET^{G810R}$ ; **C**. Best docking pose for  $RET^{I788N}$ ; **D**. Experimentally measured  $IC_{50}$  of compound **20** for the additional four RET alterations along with cell-based assay. Compound **20** (green color), key amino acid residues (yellow color), and hydrogen bond interactions (black dashed lines).

The best compound **20** was further examined for its binding mode and additional RET alterations such as  $RET^{I788N}$  (Figure 5).<sup>35–36</sup> Using the induced-fit molecular docking simulation method, we explored the binding poses and key molecular interactions of compound **20** within the active site of RET kinase (Modified RET using PDB ID: 7JU6). In the  $RET^{V804M}$  mutant, compound **20** effectively engaged the hinge residue A807 and formed critical hydrogen bonds between its amide group and D892. Additionally, the piperazine tail contributed to binding stabilization by interacting with E768. In the  $RET^{G810R}$  mutation, the compound retained a similar orientation at the hinge region, with the amine substituent at the 6-position of the

imidazopyridine core forming a key interaction with L730, whereas the tail amide continued to engage D892. Likewise, in the RET<sup>I788N</sup> mutant, compound **20** maintained hydrogen bonding with A807 via the imidazopyridine nitrogen, and the mutated asparagine residue (I788N) interacted with the carbonyl moiety. Across all the mutants, the tail amide consistently served as a critical anchor point through hydrogen bonding with D892. These *in silico* results were consistent with the *in vitro* experimental data. Clearly, compound **20** exhibited superior potency against RET<sup>V804M</sup> than the potencies against other point mutants (IC<sub>50</sub> of RET<sup>V804M</sup>: 28 nM vs IC<sub>50</sub> of RET<sup>G810R</sup>: 0.96 μM, RET<sup>I788N</sup>: 1.06 μM), and the distance from A807 also supported the experimental difference (RET<sup>V804M</sup>: 2.27 vs RET<sup>G810R</sup> & RET<sup>I788N</sup>: 2.55-2.56 Å). In the best poses, RET<sup>V804M</sup> allowed the favorable accommodation of the ester substituent at the R<sub>2</sub> position within the altered binding pocket upon close interaction with the hinge region. Meanwhile, it seems that RET<sup>G810R</sup> and RET<sup>I788N</sup> could not retain the close interaction with the hinge region as much as RET<sup>V804M</sup> because of the mutated bulky and polar arginine or asparagine side chains. Moreover, although we expected spatial compatibility between R810 residue and amine group of compound **20**, they were quite distant. Despite the hydrogen bond with N788, the combined summation of non-covalent interactions with compound **20** gave 2.56 Å as a suitable distance from the hinge region of the RET<sup>I788N</sup> mutation, which alters the structure of the αC-helix—an essential component for kinase activity and inhibitor binding.<sup>37</sup> These docking results suggest that the benefit from the R<sub>2</sub> substituent cannot be retained in these point mutations. Finally, we measured the inhibitory potencies of compound **20** against the three most important RET fusion proteins (CCDC6, KIF5B, and NCOA4). Despite the unknown 3D structure of the RET fusion proteins, compound **20** demonstrated nanomolar potency for every fusion protein (of **Figure 5D**). These findings suggest that this scaffold holds promising potential and may serve as a useful probe molecule for future mechanistic investigations of RET alterations.<sup>38</sup>

### 3. Conclusion

In this study, a series of imidazopyridine-based RET kinase inhibitors were designed and optimized to enhance both drug safety and therapeutic potential. Strategic structural modifications involved the incorporation of diverse R<sub>1</sub> group at the 6-position and the R<sub>2</sub> group introduction of cyclic tertiary, secondary aryl amides and ester at the 2-position, in combination with four different known tail groups. For the SAR optimization, the investigation of R<sub>1</sub> group, comparing heteroaryl groups, cyclic alkyl group, and halogen group revealed stereoelectronic and polarity pattern at the 6-position. In particular, the comparable activities of compounds **9h-9k** suggested further pharmacophore investigation among small R<sub>1</sub> groups to optimize the potency for RET alterations. While the 6-pyridine substituent emerged as the most favorable in terms of hERG safety profile, compound **20** demonstrated the superiority to others across both multiple RET alterations and therapeutic ratio. Molecular docking studies further supported the observed inhibitory activity by revealing the interaction distance with the hinge region within the ATP-binding site of RET kinase. In the recent future, the molecular mechanistic studies on RET fusion alterations are expected using this promising novel tool compound.

### Author contributions

View Article Online  
DOI: 10.1039/D5MD00397K

MHK conceived and designed the study and received research funding. AM synthesized the compounds using MHK's drug scaffold design. MHK, AM, VP, and SK designed the bioassay, conducted computational modeling, and analyzed the final data. MHK and AM wrote the manuscript, and MHK, AM, and VP revised it. MHK provided the molecular modelling lab and *in vitro* research facility. All the authors have read and approved the final manuscript.

### Funding sources

This study was supported by the Basic Science Research Program of the National Research Foundation of Korea (NRF), funded by the Ministry of Education, Science, and Technology (No.: **2022R1A2C2091810**). This research was also supported by a grant of the Korea Machine Learning Ledger Orchestration for Drug Discovery Project (K-MELLODDY), funded by the Ministry of Health & Welfare and Ministry of Science and ICT, Republic of Korea (No.: **RS-2024-00450691**). GL-Project of Gachon University research fund of 2021 also supported this research (No.: **GCU-202106240001**).

### Acknowledgement

The authors greatly appreciate Professor Sung-Min Ahn and Immunoforge for their valuable comments on RET drug discovery.

### Safety statement

No unexpected or unusually high safety hazards were encountered during chemical and bioassay experimentation.

### Data availability

The data supporting this article have been included as part of the Supplementary Information.

Data for this article, including Procedures of Chemical Compounds, their spectra and their bioassay data are available at Supplementary Information (submitted as DOCX).

### Conflict of interest statement

All other authors declare no conflicts of interest.

### References

- 1 A. T. Regua, M. Najjar and H.-W. Lo, *Front. Oncol.*, 2022, **12**, 932353.
- 2 D. Lipson, M. Capelletti, R. Yelensky, G. Otto, A. Parker, M. Jarosz, J. A. Curran, S. Balasubramanian, T. Bloom, K. W. Brennan, A. Donahue, S. R. Downing, G. M. Frampton, L. Garcia, F. Juhn, K. C. Mitchell, E. White, J. White, Z. Zwirko, T. Peretz, H. Nechushtan, L. Soussan-Gutman, J. Kim, H. Sasaki, H. R. Kim, S. Park, D. Ercan, C. E. Sheehan, J. S. Ross, M. T.

- Cronin, P. A. Jänne and P. J. Stephens, *Nat. Med.*, 2012, **18**, 382–384.
- 3 J. Tabata, T. Nakaoku, M. Araki, R. Yoshino, S. Kohsaka, A. Otsuka, M. Ikegami, A. Ui, S. Kanno, K. Miyoshi, S. Matsumoto, Y. Sagae, A. Yasui, M. Sekijima, H. Mano, Y. Okuno, A. Okamoto and T. Kohno, *Cancer Res.*, 2022, **82**, 3751–3762.
  - 4 A. Addeo, E. Miranda-Morales, P. Den Hollander, A. Friedlaender, H. O. Sintim, J. Wu, S. A. Mani and V. Subbiah, *Pharmacol. Ther.*, 2023, **242**, 108344.
  - 5 K. Z. Thein, V. Velcheti, B. H. M. Mooers, J. Wu and V. Subbiah, *Trends Cancer*, 2021, **7**, 1074–1088.
  - 6 G. Pecar, S. Liu, J. Hooda, J. M. Atkinson, S. Oesterreich and A. V. Lee, *Breast Cancer Res.*, 2023, **25**, 26.
  - 7 RET- My Cancer Genome. <https://www.mycancergenome.org/content/gene/ret/> (accessed 2024-03-11)
  - 8 J. F. Gainor and A. T. Shaw, *The Oncologist*, 2013, **18**, 865–875.
  - 9 V. Subbiah and G. J. Cote, *Cancer Discov.*, 2020, **10**, 498–505.
  - 10 S. Novello, R. Califano, N. Reinmuth, A. Tamma and T. Puri, *The Oncologist*, 2023, **28**, 402–413.
  - 11 K. M. Kerr, F. Bibeau, E. Thunnissen, J. Botling, A. Ryška, J. Wolf, K. Öhrling, P. Burdon, U. Malapelle and R. Büttner, *Lung Cancer*, 2021, **154**, 161–175.
  - 12 A. Maturi, K. N. V. Sastry, S. Kumar, V. Pogaku, H. J. Kwon, S.-M. Ahn and M. Kim, *ACS Med. Chem. Lett.*, 2024, **15**, 1566–1574.
  - 13 T. K. Das and R. L. Cagan, *Cell Rep.*, 2017, **20**, 2368–2383.
  - 14 C. Santos, R. Sanz-Pamplona and R. Salazar, *Ann. Oncol.*, 2018, **29**, 1340–1343.
  - 15 E. Y. Rosen, H. H. Won, Y. Zheng, E. Cocco, D. Selcuklu, Y. Gong, N. D. Friedman, I. De Bruijn, O. Sumer, C. M. Bielski, C. Savin, C. Bourque, C. Falcon, N. Clarke, X. Jing, F. Meng, C. Zimel, S. Shifman, S. Kittane, F. Wu, M. Ladanyi, K. Ebata, J. Kherani, B. J. Brandhuber, J. Fagin, E. J. Sherman, N. Rekhtman, M. F. Berger, M. Scaltriti, D. M. Hyman, B. S. Taylor and A. Drilon, *Nat. Commun.*, 2022, **13**, 1450.
  - 16 J. J. Lin, S. V. Liu, C. E. McCoach, V. W. Zhu, A. C. Tan, S. Yoda, J. Peterson, A. Do, K. Prutisto-Chang, I. Dagogo-Jack, L. V. Sequist, L. J. Wirth, J. K. Lennerz, A. N. Hata, M. Mino-Kenudson, V. Nardi, S.-H. I. Ou, D. S.-W. Tan and J. F. Gainor, *Ann. Oncol.*, 2020, **31**, 1725–1733.
  - 17 B. J. Solomon, L. Tan, J. J. Lin, S. Q. Wong, S. Hollizeck, K. Ebata, B. B. Tuch, S. Yoda, J. F. Gainor, L. V. Sequist, G. R. Oxnard, O. Gaultschi, A. Drilon, V. Subbiah, C. Khoo, E. Y. Zhu, M. Nguyen, D. Henry, K. R. Condroski, G. R. Kolakowski, E. Gomez, J. Ballard, A. T. Metcalf, J. F. Blake, S.-J. Dawson, W. Blosser, L. F. Stancato, B. J. Brandhuber, S. Andrews, B. G. Robinson and S. M. Rothenberg, *J. Thorac. Oncol.*, 2020, **15**, 541–549.
  - 18 A. M. Aronov, B. McClain, C. S. Moody and M. A. Murcko, *J. Med. Chem.*, 2008, **51**, 1214–1222.
  - 19 J.-Y. Blay and M. Von Mehren, *Semin. Oncol.*, 2011, **38**, S3–S9.
  - 20 F. H. Tan, T. L. Putoczki, S. S. Stylli and R. B. Luwor, *OncoTargets Ther.*, 2019, Volume **12**, 635–645.
  - 21 Z. Liu, Q. Lei, W. Wei, L. Xiong, Y. Shi, G. Yan, C. Gao, T. Ye, N. Wang and L. Yu, *RSC Adv.*, 2017, **7**, 27737–27746.
  - 22 B. Jin, F. Gallou, J. Reilly and B. H. Lipshutz, *Chem. Sci.*, 2019, **10**, 3481–3485.
  - 23 M. Kim, M. Kim, H. Yu, H. Kim, K. H. Yoo, T. Sim and J.-M. Hah, *Bioorg. Med. Chem.*, 2011, **19**, 1915–1923.
  - 24 E. Weisberg, P. W. Manley, W. Breitenstein, J. Brügger, S. W. Cowan-Jacob, A. Ray, B. Huntly, D. Fabbro, G. Fendrich, E. Hall-Meyers, A. L. Kung, J. Mestan, G. Q. Daley, L. Callahan, L. Catley, C. Cavazza, A. Mohammed, D. Neuberg, R. D. Wright, D. G. Gilliland and J. D. Griffin, *Cancer Cell*, 2005, **7**, 129–141.
  - 25 Y. Zhou, S. Xiang, F. Yang and X. Lu, *J. Med. Chem.*, 2022, **65**, 15540–15558.
  - 26 N. A. Meanwell, *J. Med. Chem.* 2018, **61**, 14, 5822–5880D.
  - 27 J. Baillache and A. Unciti-Broceta, *RSC Med. Chem.*, 2020, **11**, 1112–1135.
  - 28 G. Li, Y. Cheng, C. Han, C. Song, N. Huang and Y. Du, *RSC Med. Chem.*, 2022, **13**, 1300–1321.
  - 29 Y. Zhang, S. Chan, R. He, Y. Liu, X. Song, Z.-C. Tu, X. Ren, Y. Zhou, Z. Zhang, Z. Wang, F. Zhou and K. Ding, *Eur. J. Med. Chem.*, 2022, **244**, 114862.
  - 30 M. Song, *J. Med. Chem.*, 2015, **58**, 3672–3681.
  - 31 Y. Zhou, J. Kang and X. Lu, *J. Med. Chem.*, 2024, **67**, 14702–14722.
  - 32 D. Rampe and A. M. Brown, *J. Pharmacol. Toxicol. Methods*, 2013, **68**, 13–22.
  - 33 A. Garrido, A. Lepailleur, S. M. Mignani, P. Dallemagne and C. Rochais, *Eur. J. Med. Chem.*, 2020, **195**, 112290.
  - 34 M. Warmuth, S. Kim, X. Gu, G. Xia and F. Adrián, *Curr. Opin. Oncol.*, 2007, **19**, 55–60.
  - 35 T. Koga, K. Suda and T. Mitsudomi, *Cancer Sci.*, 2022, **113**, 815–827.
  - 36 R. Newton, B. Waszkowycz, C. Seewooruthun, D. Burschowsky, M. Richards, S. Hitchin, H. Begum, A. Watson, E. French, N. Hamilton, S. Jones, L.-Y. Lin, I. Waddell, A. Echaliér, R. Bayliss, A. M. Jordan and D. Ogilvie, *ACS Med. Chem. Lett.*, 2020, **11**, 497–505.
  - 37 D. Plenker, M. Riedel, J. Brägelmann, M. A. Dammert, R. Chauhan, P. P. Knowles, C. Lorenz, M. Keul, M. Bührmann, O. Pagel, V. Tischler, A. H. Scheel, D. Schütte, Y. Song, J. Stark, F. Mrugalla, Y. Alber, A. Richters, J. Engel, F. Leenders, J. M. Heuckmann, J. Wolf, J. Diebold, G. Pall, M. Peifer, M. Aerts, K. Gevaert, R. P. Zahedi, R. Buettner, K. M. Shokat, N. Q. McDonald, S. M. Kast, O. Gaultschi, R. K. Thomas and M. L. Sos, *Sci. Transl. Med.*, 2017, **9**, eaah6144.
  - 38 M. Takahashi, K. Kawai, N. Asai, *JMA J.* 2020, **3**, 175–181.



View Article Online  
DOI: 10.1039/D5MD00397K

### Data Availability Statement

The data supporting this article have been included as part of the Supplementary Information.

Data for this article, including Procedures of Chemical Compounds, their spectra and their bioassay data are available at Supplementary Information (submitted as DOCX).